Microchimica Acta (2020) 187: 637
https://doi.org/10.1007/s00604-020-04630-y

ORIGINAL PAPER

Field-effect transistor bioassay for ultrasensitive detection of folate receptor 1 by ligand-protein interaction

Yeru Liu[1] · Qiyong Cai[1] · Chaopeng Qin[2] · Yuanyuan Jin[1] · Jianxue Wang[1] · Yang Chen[1] · Yujie Ouyang[3] · Huimin Li[1] · Song Liu[1]

Received: 13 August 2020 / Accepted: 28 October 2020 / Published online: 4 November 2020

Abstract

A miniaturized and integrated bioassay was developed based on molybdenum disulfide (MoS_2) field-effect transistor (FET) functionalized with bovine serum albumin-folic acid (BSA-FA) for monitoring FOLR1. We performed the electrical test of FOLR1 within the range 100 fg/mL to 10 ng/mL, and the limit of detection was 0.057 pg/mL. The ultrahigh sensitivity of the bioassay was realized by ligand-protein interaction between FA and FOLR1, with a ligand-protein binding ratio of 3:1. The formation of FA-FOLR1 was confirmed with ELISA. The binding affinity dissociation constant K_D was 12 ± 6 pg/mL. This device can work well for FOLR1 detection in human serum, which presents its promising application in point-of-care diagnosis. This study supports the future applications of such ligand-protein-based bioassays in the clinical practices.

Keywords Folate receptor 1 · Folic acid · MoS_2 field-effect transistor · Bioassay · Ligand-protein interaction

Introduction

With the advances of bioassay technology, early diagnosis of cancer has been rapidly developed, contributing to the decline of cancer mortality. In vitro diagnostics (IVD) has realized accurate, sensitive, and specific detection of biomarkers in blood and tissues, which has become indispensable in clinical practices [1–4]. The levels of cancer-related biomarkers in blood and tissue are important indicators for determining cancer development [5]. Folate receptor 1 (FOLR1) is a glycosylphosphatidylinositol-anchored epithelial cell surface glycoprotein [6–9]. A recent study reported that the serum FOLR1 level is significantly elevated in patients with ovarian cancer, compared to that of both healthy controls and patients with benign gynecological conditions [10]. In addition, levels of FOLR1 showed better accuracy for determining ovarian cancer than other biomarkers including CA125 [11, 12]. Hence, FOLR1 may be a new promising biomarker of liquid biopsy for cancer diagnosis.

Currently, most of FOLR1 bioassays have been realized based on enzyme-linked immunosorbent assay (ELISA) [13–15]. The involvement of antibodies leads to high cost [16], due to the complex purification process and low yield. [17] Another problem is the inherent instability of antibody [18]. The antibody is susceptible to external environment such as high temperature and low pH, which results in protein denaturation and limits the consistency of detection result [19]. Taken together, it is necessary to develop new strategy for biomarker capture. Recently, Zhang et al. reported a ligand-protein recognition manner, with hyaluronic acid ligand as the probe to capture CD44 [20]. Liu et al. designed ligand-protein sensor for the detection of transferrin receptor [21]. Compared with the antibody, the ligand-based specific recognition presented attractive advantages, such as superior capture

Supplementary Information The online version contains supplementary material available at https://doi.org/10.1007/s00604-020-04630-y.

✉ Huimin Li
huiminli@hnu.edu.cn

✉ Song Liu
liusong@hnu.edu.cn

[1] Institute of Chemical Biology and Nanomedicine (ICBN), State Key Laboratory of Chemo/Biosensing and Chemometrics, College of Chemistry and Chemical Engineering, Hunan University, Changsha 410082, People's Republic of China

[2] Institute of Chemical Biology and Nanomedicine (ICBN), State Key Laboratory of Chemo/Biosensing and Chemometrics, College of Biology, Hunan University, Changsha 410082, People's Republic of China

[3] Department of Dermatology, Third Xiangya Hospital of Central South University, Changsha 410013, People's Republic of China

efficiency, high stability, facile storage, and low cost for mass production [22–24]. Notably, many researchers have testified that FOLR1 could specifically bound to folic acid (FA) and its derivatives with a high affinity [8, 25]. As a result, ligand-protein interaction like FA-FOLR1 provides an opportunity to develop new analytical platform to detect FOLR1.

Over the past decade, label-free field-effect transistor (FET) bioassays have exhibited many prominent advantages as a promising point-of-care (POC) technique, including low cost, high sensitivity, high speed, small volume, intrinsic signal amplification, and circuit integration [26–29]. Many FET-based bioassays have been widely used in tumor biomarkers, such as PSA [30, 31] and MMP-9 [19]. FET-based bioassays can accumulate hole or electron effectively on the channel materials, which can be modified with surface functionalization. Therefore, it is able to achieve rapid response to different analytes with high selectivity and sensitivity [32–34].

In general, the configuration of FET bioassay is similar to that of metal-oxide-semiconductor FET. One interface of the channel is covered by insulating membrane. However, some reports suggested that the sensitivity and selectivity of FET bioassay would be hindered by the insulating membrane [30, 35, 36]. Because the thickness of insulting membrane enlarged the distance between analyte and semiconductor. In addition, insulator plays the role of capacitor and determines the sensing current. The sensitivity of the device can be dramatically affected with the defect and dielectric constant of it [37, 38]. Recently, many membraneless FET bioassays with high sensitivity have been reported [39, 40]. For example, Liu et al. applied bare MoS_2 as the FET sensing channel to monitor DNA fragments, achieving an ultrahigh sensitivity with a limit of detection (LOD) below 100 aM [27].

Beside insulator, the dimension of the channel also plays a vital role in FET bioassay. The channel based on two-dimensional (2D) materials such as graphene and transition metal dichalcogenides have the high surface-to-volume ratio, which could supply more analyte binding sites and improve the sensitivity of the bioassay [41]. However, although graphene provides high mobility and sensing layer with atomic thickness, the sensitivity and response of graphene-based bioassay would be seriously restricted due to the absence of band gap and small on/off current ratio [42, 43]. Additionally, when utilizing 2D materials in bioassay, we must consider the toxicity of the materials. For example, some research results indicated that the 2D materials such as WSe_2 [44], VTe_2 [45], and $NbTe_2$ [46] showed poor biocompatibility. Alternatively, MoS_2 is one of the most extensively studied 2D semiconducting materials. The development in MoS_2-based bioassays ascribed to the inherent advantages of MoS_2, such as exceptional biocompatibility [47], easy modification [48], ultrafast saturable absorption [49], high on/off ratios, and high surface-to-volume ratio [50]. In particular, mechanically exfoliated MoS_2 sheets with minimal defects can achieve relatively high mobility, on/off current ratio, and current level in FETs [51]. Until now, many ultrasensitive membraneless FET bioassays prepared with mechanically exfoliated MoS_2 have been reported for the detection of PSA [52] and IgG [53]. However, few studies have been performed on the integration of membraneless MoS_2 FET with ligand-protein interaction for the detection of FOLR1.

In this work, a membraneless MoS_2 FET bioassay based on the ligand-protein interaction has been firstly prepared for FOLR1 detection. In this bioassay, BSA-FA is serving as the probe, that is, FA ligand as the capture component and BSA as the conjugate molecule to improve the biocompatibility and water solubility. The specific binding between BSA-FA and FOLR1 could mediate electrical signal and give ultrahigh sensitivity of the bioassay. A good linearity for threshold voltage (V_{th}) vs FOLR1 concentrations can be observed, with an extracted LOD of 0.057 pg/mL. In addition, a nonaqueous environment measurement has been applied in this study, which not only simplified the preparation process but also avoided the ionic screening effects.

Experimental section

Materials and reagents

Molybdenum disulfide (MoS_2) was purchased from Resemi (Suzhou, China). 1-Pyrenebutanoic acid N-hydroxysuccinimidyl ester (PASE, 95%) was obtained from Sigma-Aldrich (China). Bovine serum albumin (BSA, 98%) was purchased from J&K (China). Bovine serum albumin-folic acid (BSA-FA) was purchased from Cusabio (Wuhan, China, www.cusabio.cn). Recombinant human FOLR1 protein (95%) and human FOLR1 antibody were obtained from R&D (USA).

The fabrication of MoS_2 device

Few-layer MoS_2 flakes were produced by mechanical exfoliation and then transferred onto p++Si substrate with 300 nm oxides via Scotch tape. That is, we first adhered adhesive tape to the surface of the bulk materials and peeled it off. Then, press the tape firmly yet gently onto the silicon wafer piece, peeling it off, and the silicon wafer washed with isopropanol to clean the organic residue. The wafer can now be viewed under the optical microscope. The thickness of MoS_2 materials can be roughly estimated by the color of it, which will vary depending on the microscope. Finally, the few-layer MoS_2 flakes were produced. TEM copper grid was then used to make patterns of electrodes on the assurance MoS_2 flakes. Subsequently, the source and drain electrodes (In/Au 5/50 nm) were formed via vacuum coating machine.

Thermal evaporation was carried out at the rate of 0.2 Å/s in the study. Removing the TEM copper grid template and the source and drain electrodes connected by the material were constructed into field-effect transistor device. The detailed preparation process is shown in Scheme S1 in the Electronic Supplementary Materials. The device was annealed at 200 °C for 2 h in mixed gases (Ar/H_2, 100/10 sccm) to improve the contacts between MoS_2 and electrodes, as well as removing residual organic contaminants during fabrication.

Immobilization of BSA-FA

To anchor BSA-FA on the channel of the MoS_2 FET, the device was firstly immersed into 5 mMol 1-pyrenebutanoic acid succinimidyl ester (PASE) in DMF and incubated for 2 h. The PASE-coated device was washed sequentially in DMF, ethanol, and deionized (DI) water. Then, 10 μL of 100 μg/mL BSA-FA in 1× PBS (pH 7.2–7.4) was dropped on the chip and incubated overnight at 4 °C in a refrigerator for conducting the chemistry reaction between BSA-FA and PASE. The FET bioassay was rinsed with 1× PBS, DI water in order to remove the unbound BSA-FA. After that, the device was blocked with BSA solution (50 μg/mL, 10 μL) for 1 h to occupy nonspecific binding sites, followed by washing with 1× PBS, DI water, and drying with N_2. Ultimately, the device was stored at 4 °C in a refrigerator for further use.

Detection of FOLR1 in PBS

The electrical response of the FET was measured with a semiconductor parameter analyzer (Keithley, 2643B) and a probe station (Cascade Microtech, MPS 150) at room temperature in air. In the measurements, 10 μL of FOLR1 in 1× PBS (pH 7.2–7.4) with a gradually increased concentration ranged from 100 fg/mL to 10 ng/mL was added on the device surface and incubated for 20 min at room temperature. Then, the chip was rinsed with 1× PBS, DI water and dried with N_2. The MoS_2 FET bioassay measurement was carried out after various concentrations of FOLR1 treatment. The transfer curves of the FET bioassay were measured with a silicon substrate as the back gate and a fixed source-drain voltage $V_{ds} = 0.5$ V. The bioassay based on antibody-antigen mode for detecting FOLR1 was carried out in the same condition. The only difference is that BSA-FA is replaced by anti-FOLR1.

Detection of FOLR1 in human serum sample

Serum samples were volunteered by Qiyong Cai, the author of this article. He is 29 years old and in good health. The obtained serum samples were stored at − 80 °C until use. Human serum samples were treated by centrifugation at 2000×*g* for 10 min. The serum was diluted 10-fold. The recovery experiment was performed toward 10-fold diluted serum spiked with the different concentrations (50 pg/mL, 100 pg/mL, 200 pg/mL) of FOLR1. And then, six different concentrations of FOLR1 in 10-fold diluted serum from 100 fg/mL to 10 ng/mL were dissolved. All electrical measurement of MoS_2 FET bioassay for detection of various FOLR1 in human serum remains the same as that described in PBS.

Selectivity and stability investigation

To determine the specificity of the bioassay for FOLR1, some common proteins were investigated, including carcinoembryonic antigen (CEA), squamous cell carcinoma antigen (SCCA), and P53, and the concentration is 10 ng/mL. The measurement procedure remains the same as the detection of FOLR1. The stability of the bioassay was conducted by monitoring the signal response to 10 pg/mL FOLR1 three times daily, and then the devices were stored at 4 °C in a refrigerator.

BSA-FA-based ELISA for the detection of FOLR1

The 1 mg/mL BSA-FA was diluted to 10 μg/mL with 50 mMol carbonate buffer. 100 μL of BSA-FA solution (10 μg/mL) was added in each well of 96 well polystyrene plate and coated at 4 °C overnight. The coating solution was removed and the plate was washed twice with 200 μL of 1× PBS per well. Then, 200 μL of blocking buffer (0.5% BSA solution) was added in each well to block the remaining protein-binding sites for 2 h at room temperature. The plate was washed twice with 1× PBS. Next, 100 μL of FOLR1 proteins (0 ng/mL, 1 ng/mL, 10 ng/mL, and 100 ng/mL) was added and then captured with the pre-coated FA. Because the recombination FOLR1 protein contained His tag, mouse anti-His monoclonal antibody was served as the detection antibody. Then, horseradish peroxidase–labeled goat anti-mouse secondary antibody was added and reacted with the detection antibody. Finally, the results were developed with tetramethylbenzidine (TMB) as colorimetric substrate. Absorbance was measured in a plate reader (SPARK, 10M, TECAN).

Characterization

To confirm the functionalization of all molecules onto the MoS_2 surface, Raman spectroscopy was performed using invia-reflex system with a 532 nm excitation laser. The surface topography of MoS_2 channel, functionalized with biomolecules in stepwise, was carried out using tapping-mode atomic force microscope (AFM) (Bruker Dimension Icon). To further investigate the immobilization of BSA-FA, X-ray photoelectron spectroscopy (XPS) spectra of pristine and BSA-FA-immobilized MoS_2 were obtained by using AXIS SUPRA system with Al X-ray source (Kα 1486.6 keV).

Results and discussion

Fabrication of MoS_2 FET bioassay

The fabrication procedure of the MoS_2 FET bioassay is illustrated in Fig. 1. Prior to surface modification, back gate MoS_2 FET was prepared. In brief, mechanically exfoliated few-layer MoS_2 was transferred onto SiO_2/Si substrate, where SiO_2 with the thickness of 300 nm functioned as the gate dielectric, and the p-doped Si worked as the back gate. The Raman spectra with the E^1_{2g} and A_{1g} modes were observed at 380 and 404 cm^{-1}, respectively, which suggests that the exfoliated material is indeed few-layer MoS_2, as shown in Fig. S1. Source/drain electrodes (In/Au 5/50 nm) were patterned on MoS_2 by thermal evaporation. Aiming to achieve superior sensing performance and high field-effect mobility (μ = 10–20 cm^2V^{-1} s^{-1}) [54], the large surface area of the channel with a width of 12 μm and the thickness of MoS_2 film ranged from 5 to 15 nm was chosen (Fig. S2). AFM image clearly showed the exact thickness of MoS_2 is 8 nm. Functionalization was performed with layer-by-layer assembling. Firstly, PASE molecules were attached onto MoS_2 surface as the linker [55]. Then, the amino group of BSA-FA was reacted with carbonyl group of PASE via the N-hydroxy succinimide (NHS) chemistry for immobilizing BSA-FA [40, 43]. Next, BSA was applied as the blocking agent to prevent nonspecific binding between FOLR1 and substrate material, as well as blocking the excess carbonyl groups. Finally, the assay was applied in detecting different concentrations of FOLR1, which is specifically bound to BSA-FA. The variation of electrical conductance was recorded synchronously.

Characterization of MoS_2 FET bioassay

To validate the functionalization process, the MoS_2 flake was characterized by AFM in a stepwise manner. Compared to the pristine MoS_2 film surface topography, the root-mean-squared (RMS) roughness of the immobilized BSA-FA increased from 0.217 to 1.54 nm, suggesting that BSA-FA is successfully bonded to PASE (Fig. 2a, b). The RMS roughness of the sample slightly increased to 1.58 nm after being blocked by BSA, indicating that nonspecific binding sites are blocked well (Fig. 2c). Lastly, the FOLR1 protein was introduced into the MoS_2 channel (Fig. 2d). The RMS roughness increased to 1.78 nm. Here, the value of RMS roughness of each step was estimated from the full size of the image. Moreover, as shown in Fig. 2d, in contrast to previous steps, the number of bright spots is significantly increased, indicating an increased average height of the device surface. The topographic images of stepwise modification are shown in Fig. S3. From AFM images, the average height increased by 1.2 nm after the device was incubated in FOLR1 solution (Fig. S3d), which is lower than that of FOLR1. Because the molecular weight of FOLR1 is roughly 25.4 kDa in this work. This may be due to the diversity of binding directions of FOLR1 and BSA-FA and measurement errors. These results clearly identified that the FOLR1 proteins bond to BSA-FA immobilized on the FET device.

The electrical characteristics in all steps were also measured to further testify the functionalization of the MoS_2 FET. After the binding of charged biomolecules on bioassay channel, the signal transduction can be altered by electrostatic gating and/or charge transfer, inducing the

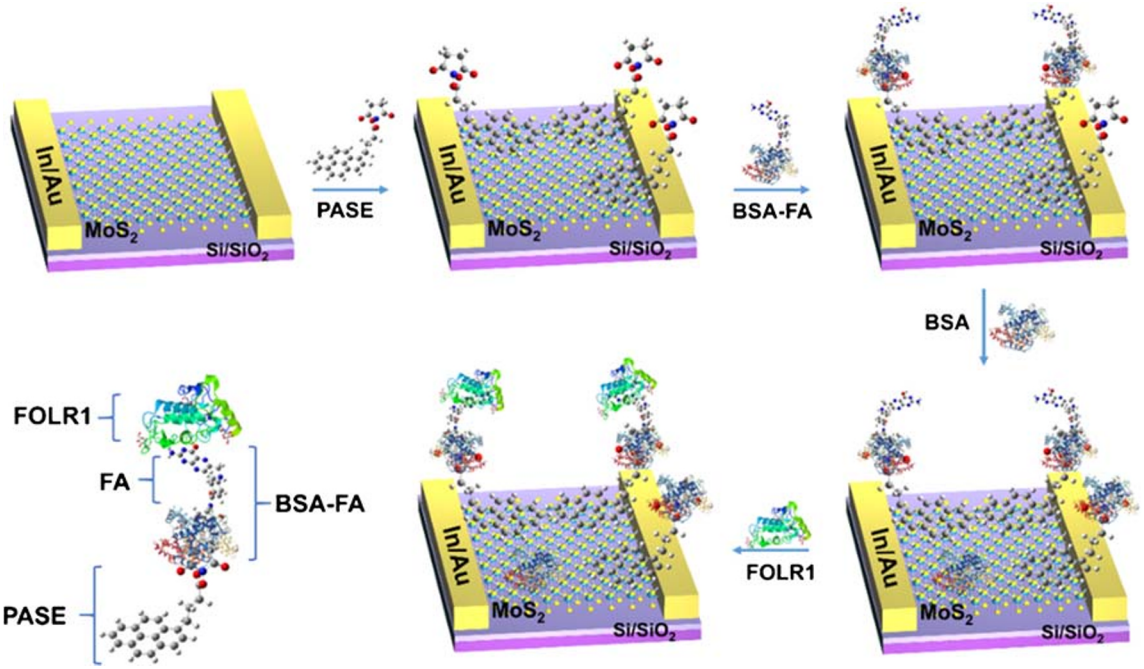

Fig. 1 Schematic illustration of the preparation process of MoS_2 FET bioassay for FOLR1 detection

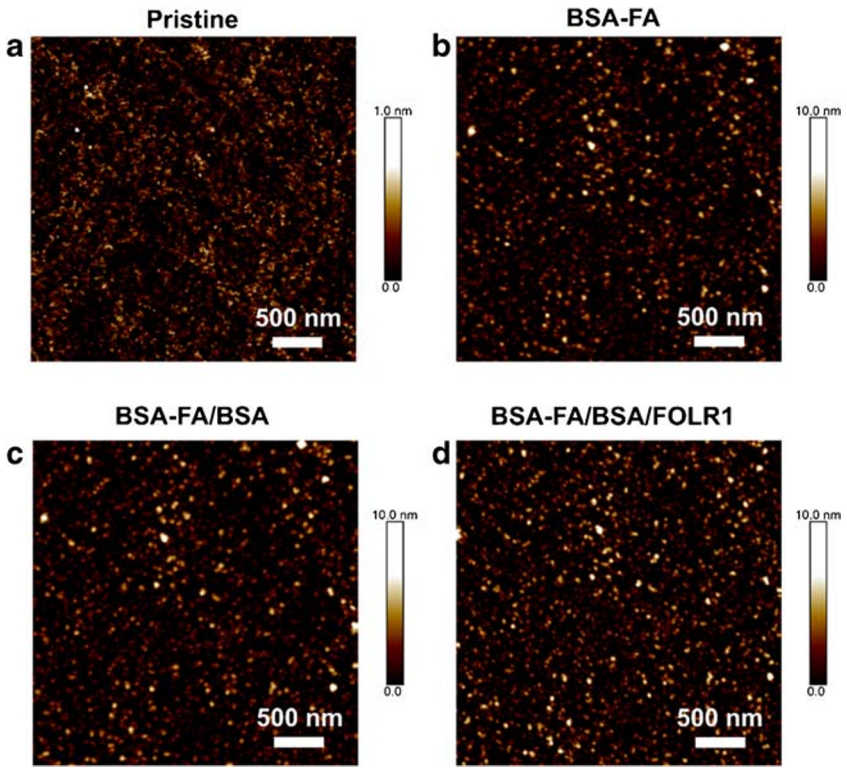

Fig. 2 Surface roughness of AFM images of the same device with pristine MoS_2 (**a**) and sequentially immobilizing with BSA-FA (**b**), blocking with BSA (**c**) and treating with FOLR1 (**d**)

changes of sensing current. During the experiment, all biomolecules were in 1× PBS (pH 7.2~7.4). The isoelectric point (pI) of BSA-FA, BSA, and FOLR1 is ~4.7, ~4.7, and ~8.2, respectively, indicating that BSA-FA and BSA are negatively charged, and FOLR1 is positively charged in the PBS. Notably, both the theory of "pH-memory" and many studies prove that the biomolecules retained ionization state in a nonaqueous environment [31]. Therefore, as depicted in Fig. 3a, the stepwise transfer characteristics of MoS_2 FET bioassay were observed under nonaqueous environment. The source-drain current (I_{ds}) was measured as a function of back gate voltage (V_{gs}) from − 60 to 60 V with a set drain voltage (V_{ds}) of 0.5 V.

As shown in Fig. 3b, step 1, the pristine MoS_2 FET showed typical n-type conductance, consistent with previously reported results [19]. In addition, the linear output curve of the device is presented in Fig. S4, demonstrating the presence of Ohmic contact between In and MoS_2. After dropping PASE solution onto the device, a positive shift of threshold voltage (V_{th}) from 8.18 to 10.3 V was obtained (Fig. 3b, step 2), suggesting the p-type doping of PASE. Furthermore, Raman spectroscopy was performed before and after PASE coupled

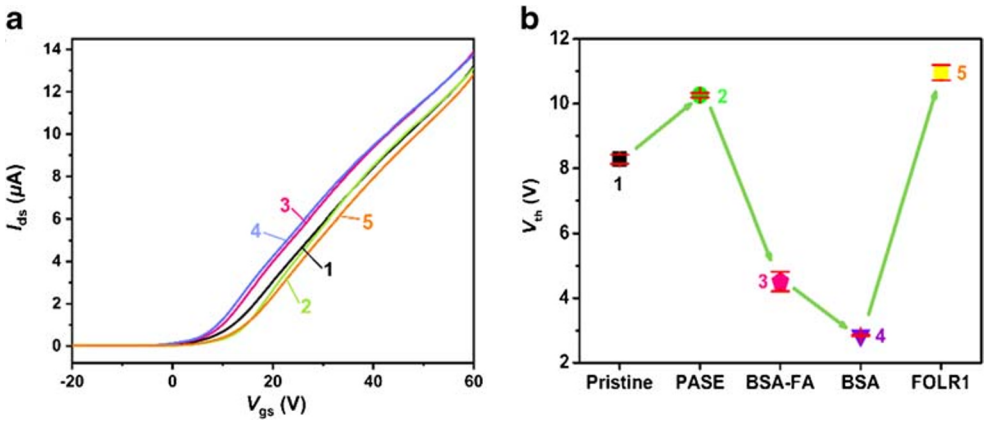

Fig. 3 Transfer curves (**a**) and V_{th} changes (**b**) of the MoS_2 FET bioassay functionalization process in a stepwise manner: (1) pristine, (2) pristine + PASE, (3) pristine + PASE + BSA-FA, (4) pristine + PASE + BSA-FA + BSA, (5) pristine + PASE + BSA-FA + BSA + FOLR1 (100 pg/mL). Transfer characteristics of the bioassay were obtained with V_{gs} various from − 60 to 60 V and V_{ds} = 0.5 V (in order to show the current change more clearly, the data with V_{gs} various from − 60 to − 20 V was omitted)

to MoS_2. As shown in Fig. S5, the clear blue-shift of Raman signatures was obtained as compared with pristine MoS_2, which confirms the p-type doping effect of PASE [56]. The result is similar to the PASE-doped graphene in other studies [57]. When negatively charged BSA-FA was reacted with PASE, there is a considerable left-shifted V_{th} (Fig. 3b, step 3). This can be interpreted by improved surface negative charge density of MoS_2 and increased electron injection to the MoS_2 channel.

Notably, in our nonaqueous system, electrostatic gating effect induced by the weakly charged BSA-FA can be ignored [58]. Additionally, a previous study reported that electrons of protein could be directly transferred into graphene or carbon nanotube via the amine group [39]. For MoS_2, we postulate that the immobilization of BSA-FA could generate n-type doping effect on MoS_2, and, consequently, increase the on-current. In other words, negatively charged biomolecules act as electron donors causing left-shifted V_{th}, and increasing I_{ds}. This change is consistent with previously reported results [40, 57, 58]. To further prove the functionalization of BSA-FA, we performed XPS measurement because the N-content of BSA-FA can induce the changes of N 1s peaks. As shown in Fig. S6, in contrast to the pristine MoS_2, an additional peak area and increased peak intensity was observed in N 1s core level, which is assigned to the immobilization of BSA-FA on the device. After the device was blocked in BSA (50 μg/mL) solution, V_{th} showed a relatively small negative shift (Fig. 3b, step 4), implying that the amount of the immobilized BSA is extremely lower than that of BSA-FA. Finally, the positively charged FOLR1 (100 pg/mL) specifically combined with BSA-FA, and the value of V_{th} is positively shifted to 10.8 V (Fig. 3b, step 5). It may be resulted from the opposite charge between BSA-FA and FOLR1, in which FOLR1 decreased negative charge density on MoS_2. As a result, the electrons transfer in MoS_2 is significantly hindered by FOLR1, and consequently, the n-type doping effect of BSA-FA is weakened. Thereby, FOLR1 functioned as p-type dopant and decreased the on-current. To further identify the immobilization of BSA-FA, BSA, and FOLR1, the Raman spectroscopy was performed (Fig. S7). After the stepwise BSA-FA and BSA treatment, as shown in Fig. S7b, the frequency of the E^1_{2g} and A_{1g} mode gradually decreases, indicating that BSA-FA and BSA fixed on the device exhibits the n-type doping effect [59]. When the device was incubated in FORL1 solution, the enhancement of Raman mode intensity proves the p-type doping effect [60]. The above results certified that the MoS_2 FET bioassay was successfully fabricated in a stepwise manner, in good agreement with AFM measurement result.

Feasibility study

Many researchers have reported that FOLR1 presented high affinity with FA and its derivatives [8, 61]. We have tried to verify whether the increased roughness and shifted V_{th} after the FOLR1 combination are ascribed to the specific binding of FOLR1 to BSA-FA. Conventional ELISA was performed with various concentrations of FOLR1 ranged from 1 to 100 ng/mL. As shown in Fig. 4, optical density (OD) value was increased with the improved concentration of FOLR1, and the color of the solution was changed from colorless to yellow correspondingly (Fig. 4, inset). These results prove that BSA-FA can specifically bind to FOLR1, instead of simple charge interaction. They also demonstrated that the small molecular FA can be alternative of antibody for the detection of FOLR1.

Electrical response of various FOLR1 concentrations in PBS

In order to obtain the optimal incubation time of the target molecules, the specific binding curve was plotted. Fig. S8 presents the variation of V_{th} with binding time, at a fixed FOLR1 concentration of 1 ng/mL. The dynamic equilibrium of binding reaction was completed after 20 min. Thus, the incubation time is set as 20 min for various concentrations of FOLR1. In addition, the buffer is also a critical consideration for the specific binding, and 1× PBS serving as the optimal buffer. The result is related to Debye screening length, namely the charged molecules on a certain length scale (Debye length λ_D) would be screened by counterions. Many studies reported that increased buffer ionic strengths yield a reduced Debye length, according to the formula $\lambda_D = 0.32 (I)^{-0.5}$, where I is the ionic strength of the buffer solution [62]. Thus, the Debye length of 1× PBS (~0.7 nm) buffer solution is shorter compared to that of 0.1× PBS (~2.3 nm) and 0.01× PBS (~7.3 nm). The shorter Debye length may allow the screening of more charges [63], thus promoting the specific binding and improving the sensitivity of bioassay.

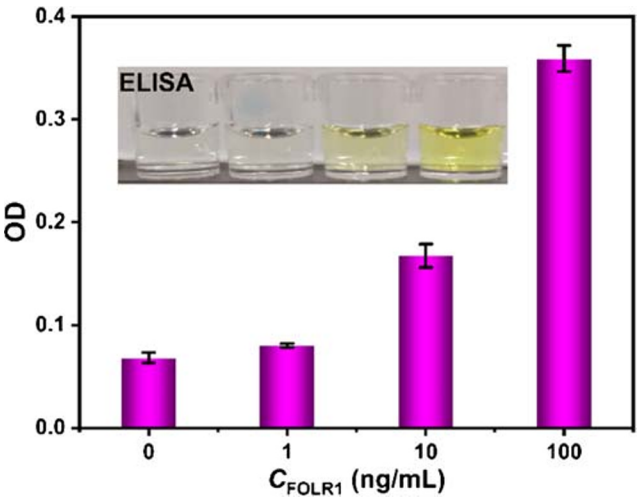

Fig. 4 Various concentrations of FOLR1 (1 ng/mL, 10 ng/mL, and 100 ng/mL) were monitored by BSA-FA-based ELISA

The detection of different concentrations of FOLR1 was performed by MoS_2 FET bioassay in a nonaqueous environment. As shown in Fig. 5a, in the range between 100 fg/mL and 10 ng/mL, the I_{ds}-V_{gs} curves were obtained with V_{gs} various from − 60 to 60 V and $V_{ds} = 0.5$ V. The bioassay blocked with BSA and then immersed into PBS to establish a baseline current. After incubating with positively charged FOLR1, the I_{ds} was decreased and the V_{th} was gradually shifted to the positive gate voltage with increased concentrations (Table S1), representing p-type doping effects on MoS_2. Moreover, as the concentration further increased to 10 ng/mL, the electrical signal became stable, suggesting binding sites become saturated. The same results were obtained independently from three different FET bioassays (Fig. S9).

To effectively assess the quantification performance of this bioassay, assay response is defined as ΔV_{th} and calibrated as $\Delta V_{th} = V_{th}$ (C) − V_{th} ($n = 0$), indicating the variation of V_{th} between the concentration of FOLR1 and the baseline. As shown in Fig. 5b, the relationship between the calibrated response ΔV_{th} and FOLR1 concentration was summarized (the data in Fig. 5a converted to 5b). When the concentration of FOLR1 is above 1 ng/mL, ΔV_{th} became stable, indicating that all binding sites had theoretically reacted with it and the assay signal reached saturated. Moreover, a great detection linearity for FOLR1 with the concentration spanned from 100 fg/mL to 1 ng/mL was observed (Fig. 5b, Inset). The regression equation is $\Delta V_{th} = 1.17 \times \lg C_{FOLR1} - 1.26$, and the correlation coefficient is 0.9988. The standard deviation (RSD) was calculated from measurements of three devices ($n = 3$), which is not significantly deviated from the mean value (< 6%) at different levels. Above result suggested high reproducibility for MoS_2 bioassay. Furthermore, the LOD was estimated to be 0.057 pg/mL ($S/N = 3$), representing high sensitivity of FET bioassay.

Compared with some presented detection methods (Table S2), the developed MoS_2-based FET bioassay exhibits lower LOD, higher sensitivity, and faster response time. These results supported the applications of FET bioassay for the ultrasensitive and quantitative detection of FOLR1. In addition, the predominant detection performance is also attributed to the strong binding affinity between FA and FOLR1. Figure 5c shows $C_{FOLR1}/\Delta V_{th}$ plotted as a function of various FOLR1 concentrations, which can be described by Hill-Langmuir equation [33, 40, 57]:

$$\frac{C_{FOLR1}}{\Delta V_{th}} = \frac{C_{FOLR1}}{\Delta V_{th,max}} + \frac{K_D}{\Delta V_{th,max}} \quad (1)$$

where $\Delta V_{th,\,max}$ is the maximum change of the V_{th}, C_{FOLR1} is the concentration of FOLR1, and K_D is the binding affinity dissociation constant for BSA-FA and FOLR1. The K_D value was estimated to be 12 ± 6 pg/mL, lower than that of currently reported antibody-antigen bioassay [64], indicating the relatively high affinity between the small molecular ligand FA and FOLR1. To further prove FA ligand gives ultrahigh sensitivity and quantification of the device, the FET bioassay in antibody-antigen mode for detecting FOLR1 was performed. Firstly, the reaction of dynamic equilibrium between anti-FOLR1 and FOLR1 was carried out. The binding stability was completed after 50 min (Fig. S10), which is longer than that of ligand-antigen mode. Then, the transfer characteristics of the device were obtained, as shown in Fig. S11a, and the current decreases with increasing FOLR1 concentration. A great detection linearity for FOLR1 with the concentration ranged from 100 fg/mL to 1 ng/mL was observed, and the K_D value was also estimated to be 14 ± 7 pg/mL, as shown in Fig. S11b and S11c. By contrast, the K_D value is lower than that of antibody-antigen FET bioassay, which may be due to multiple binding sites between FA and FOLR1 [65]. This result further validates the high sensitivity of the FET bioassay. Beside lower K_D value, the ultrasensitive and fast detection for FOLR1 is also attributed to nonaqueous measurement environment. Because Debye screening length made few effects on detection, and avoided the leakage (less than 0.1 nA) induced by the ions in buffer solution.

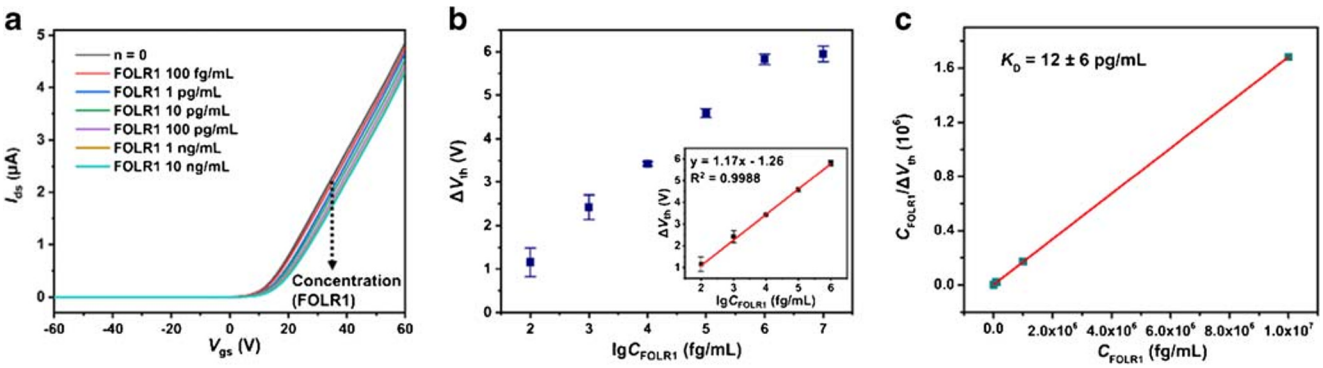

Fig. 5 **a** Transfer curves of the MoS_2 FET bioassay in response to various FOLR1 concentrations in 1× PBS. **b** Calibrated response ΔV_{th} versus the FOLR1 concentration for the MoS_2-based bioassay. The inset showed a linear relationship between ΔV_{th} and various concentrations of FOLR1. **c** A least-squares fit to Hill-Langmuir equation, yielding the K_D of 12 pg/mL

For verifying that the obtained V_{th} shift can be indeed mediated by FOLR1, several control experiments were set and conducted. As depicted in Fig. S12a, the electrical response of bioassay without BSA-FA was recorded to demonstrate nonspecific reaction between BSA and FOLR1. The addition of various concentrations of FOLR1 to the device presented negligible change of transfer curves, suggesting no noticeable nonspecific binding between them. In addition, owing to the nonaqueous measurement condition, bioassay was immersed into 1× PBS before the immobilization of FOLR1, and then dried with N_2. As shown in Fig. S12b, the current signal only slightly changed, revealing the buffer made no significant interfering effects during the stepwise modification. The above results supported the reliability of our detection system.

Selectivity and stability

The selectivity and stability of MoS_2 FET bioassay in complex media was investigated to further evaluate the practicality of the method. In selectivity test, the sensing signal of potential interference factors was recorded, such as carcinoembryonic antigen (CEA), squamous cell carcinoma antigen (SCCA), and P53. Negligible V_{th} shifts (ΔV_{th}) were observed when the device was exposed to the above interferences. The concentration of CEA, SCCA, and P53 (10 ng/mL) is ten times that of FOLR1 (1 ng/mL), while a significant ΔV_{th} was observed after the introduction of only 1 ng/mL FOLR1. The selectivity of the device is further tested with the mixed solutions, including CEA (10 ng/mL) + FOLR1 (1 ng/mL), SCC (10 ng/mL) + FOLR1 (1 ng/mL), and P53 (10 ng/mL) + FOLR1 (1 ng/mL). For above solutions, acceptable difference of ΔV_{th} was observed (Fig. 6a), showing the excellent selectivity of the MoS_2 FET bioassay for FOLR1 detection. In addition, the stability of the bioassay was examined (Fig. 6b). The BSA-FA functionalized device was preserved at 4 °C in refrigerator for different days and the ΔV_{th} response to 10 pg/mL FOLR1 was recorded. After the storage for 7 days, the ΔV_{th} response still retained 90% of its initial response ($\Delta V_{th,\ 0}$). It indicated acceptable storage stability of this FET bioassay. However, bioassay platform with better stabilization still poses challenges to mass production.

Electrical response of various FOLR1 concentrations in serum

The potential applicability of the bioassay as POC device was validated in human serum. The FOLR1 with different concentrations (50 pg/mL, 100 pg/mL, 200 pg/mL) were added into 10-fold diluted serum, and the recoveries of FOLR1 were estimated to be 98%, 102%, and 95.5%, respectively (Table S3). These results suggest that the developed bioassay is reliable for detecting FOLR1. The electrical response of the bioassay corresponding to the detection of different concentrations of FOLR1 in 10-fold diluted human serum is depicted in Fig. S13a. Treatment process and measurement condition are maintained in the PBS buffer. The sensing linearity of the FET device between calibrated response ΔV_{th} and FOLR1 concentration (from 100 fg/mL to 1 ng/mL) was observed (Fig. S13b). The linear regression equation of bioassay was $\Delta V_{th} = 1.49 \times \lg C_{FOLR1} - 0.46$ (inset in Fig. S13b), and the LOD was extracted to 0.086 pg/mL ($S/N = 3$). The error bar was calculated from three devices. The sensing response of different FET devices to various FOLR1 concentrations is similar, as displayed in Fig. S14. Importantly, the detection performance in human serum is comparable to that of in PBS buffer. The bioassay exhibited ultrahigh sensitivity and satisfactory selectivity in the real human serum. This satisfactory result provides the potential to cell capture for disease

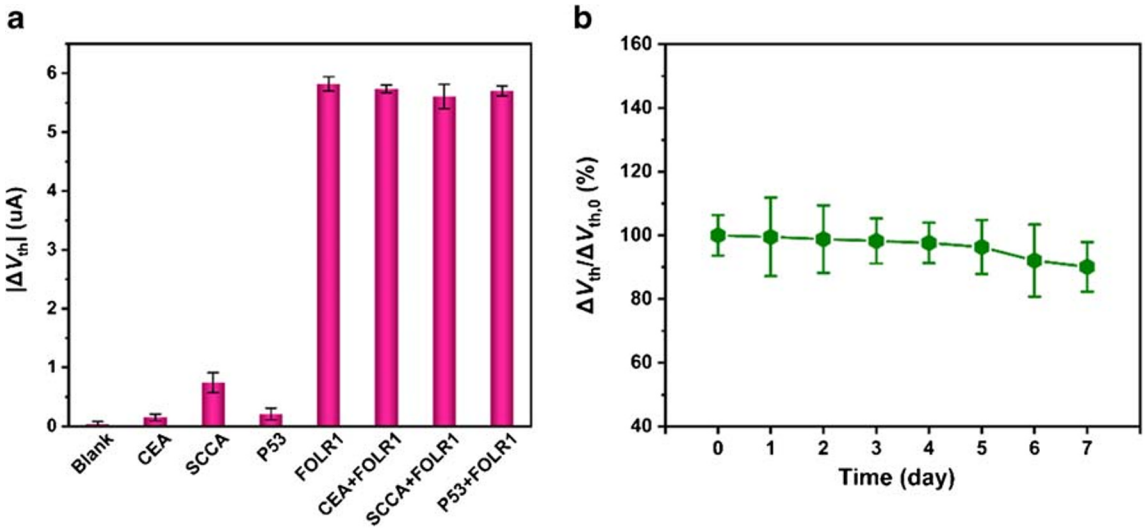

Fig. 6 **a** Selectivity of MoS_2 FET bioassay for FOLR1 from a series of interference factors. **b** Stability test of the MoS_2 FET bioassay after the storage for 7 days

diagnosis in the future [66–68]. Therefore, the MoS_2 FET bioassay showed promising application prospects in future clinical diagnosis.

Conclusion

We have successfully realized the detection of FOLR1 by an MoS_2 FET bioassay for the first time in a nonaqueous environment. Based on the charge doping, the specific binding between small molecular FA and FOLR1 with a high affinity produced significant conductance variation on the membraneless MoS_2 channel. The shifted V_{th} was obtained with various concentrations of FOLR1, in a linear relationship. The high electivity and reliability were observed based on the results of selectivity and control experiments. We have also demonstrated the label-free MoS_2 bioassay platform can be applicable to the detection of FOLR1 in serum. In view of the importance of the detection of biomarkers for determining cancer development, the FET bioassay based on ligand-protein interaction provides the possibility of IVD testing. However, the poor stability of this method can be a challenge for mass production. Thus, further improving the performance of the device will be conducive to the real-life application of it.

Funding This study was financially supported by the National Natural Science Foundation of China (No. 21975067), Technology Innovation Program of Hunan Province (No. 2018RS3060), and Fundamental Research Funds for the Central Universities from Hunan University.

Compliance with ethical standards

Conflict of interest The authors declare no competing financial interests.

References

1. Goble JA, Rocafort PT (2015) Point-of-care testing: future of chronic disease state management? J Pharm Pract 30(2):229–237. https://doi.org/10.1177/0897190015587696
2. Luppa PB, Bietenbeck A, Beaudoin C, Giannetti A (2016) Clinically relevant analytical techniques, organizational concepts for application and future perspectives of point-of-care testing. Biotechnol Adv 34(3):139–160. https://doi.org/10.1016/j.biotechadv.2016.01.003
3. Rohr U-P, Binder C, Dieterle T, Giusti F, Messina CGM, Toerien E, Moch H, Schäfer HH (2016) The value of in vitro diagnostic testing in medical practice: a status report. PLoS One 11(3): e0149856. https://doi.org/10.1371/journal.pone.0149856
4. Holland M, Kraght P, Akbas N, Budd J, Klee G (2017) Improved statistical methods for evaluation of stability of in vitro diagnostic reagents. Stat Biopharm Res 9(3):272–278. https://doi.org/10.1080/19466315.2017.1305287
5. Tseng Y-J, Huang C-E, Wen C-N, Lai P-Y, Wu M-H, Sun Y-C, Wang H-Y, Lu J-J (2019) Predicting breast cancer metastasis by using serum biomarkers and clinicopathological data with machine learning technologies. Int J Med Inf 128:79–86. https://doi.org/10.1016/j.ijmedinf.2019.05.003
6. Shi H, Guo J, Li C, Wang Z (2015) A current review of folate receptor alpha as a potential tumor target in non-small-cell lung cancer. Drug Des Devel Ther 9:4989–4996. https://doi.org/10.2147/DDDT.S90670
7. O'Shannessy DJ, Yu G, Smale R, Fu Y-S, Singhal S, Thiel RP, Somers EB, Vachani A (2012) Folate receptor alpha expression in lung cancer: diagnostic and prognostic significance. Oncotarget 3(4):414–425. https://doi.org/10.18632/oncotarget.489
8. Nunez MI, Behrens C, Woods DM, Lin H, Suraokar M, Kadara H, Hofstetter W, Kalhor N, Lee JJ, Franklin W, Stewart DJ, Wistuba II (2012) High expression of folate receptor alpha in lung cancer correlates with adenocarcinoma histology and mutation. J Thorac Oncol 7(5):833–840. https://doi.org/10.1097/JTO.0b013e31824de09c
9. Bueno R, Appasani K, Mercer H, Lester S, Sugarbaker D (2001) The α folate receptor is highly activated in malignant pleural mesothelioma. J Thorac Cardiovasc Surg 121(2):225–233. https://doi.org/10.1067/mtc.2001.111176
10. Leung F, Bernardini MQ, Brown MD, Zheng Y, Molina R, Bast RC, Davis G, Serra S, Diamandis EP, Kulasingam V (2016) Validation of a novel biomarker panel for the detection of ovarian cancer. Cancer Epidemiology Biomarkers & Prevention 25(9): 1333–1340. https://doi.org/10.1158/1055-9965.EPI-15-1299
11. Kurosaki A, Hasegawa K, Kato T, Abe K, Hanaoka T, Miyara A, O'Shannessy DJ, Somers EB, Yasuda M, Sekino T, Fujiwara K (2016) Serum folate receptor alpha as a biomarker for ovarian cancer: implications for diagnosis, prognosis and predicting its local tumor expression. Int J Cancer 138(8):1994–2002. https://doi.org/10.1002/ijc.29937
12. Leung F, Dimitromanolakis A, Kobayashi H, Diamandis EP, Kulasingam V (2013) Folate-receptor 1 (FOLR1) protein is elevated in the serum of ovarian cancer patients. Clin Biochem 46(15): 1462–1468. https://doi.org/10.1016/j.clinbiochem.2013.03.010
13. Human FOLR1 ELISA Kit. https://www.raybiotech.com/human-folr1-elisa-kit/
14. Human Folate Receptor Alpha (FOLR1) ELISA kit. http://www.cusabio.cn/product/ELISA Kit/Human Folate receptor alpha(FOLR1) ELISA kit-78958.html
15. Human FOLR1 Quantikine ELISA Kit. https://www.rndsystems.com/cn/products/human-folr1-quantikine-elisa-kit dflr10
16. Sakamoto S, Putalun W, Vimolmangkang S, Phoolcharoen W, Shoyama Y, Tanaka H, Morimoto S (2018) Enzyme-linked immunosorbent assay for the quantitative/qualitative analysis of plant secondary metabolites. J Nat Med 72(1):32–42. https://doi.org/10.1007/s11418-017-1144-z
17. Bergmann-Leitner ES, Mease RM, Duncan EH, Khan F, Waitumbi J, Angov E (2008) Evaluation of immunoglobulin purification methods and their impact on quality and yield of antigen-specific antibodies. Malar J 7:129. https://doi.org/10.1186/1475-2875-7-129
18. Vermeer AWP, Norde W (2000) The thermal stability of immunoglobulin: unfolding and aggregation of a multi-domain protein. Biophys J 78(1):394–404. https://doi.org/10.1016/S0006-3495(00)76602-1
19. Park H, Lee H, Jeong SH, Lee E, Lee W, Liu N, Yoon DS, Kim S, Lee SW (2019) MoS_2 field-effect transistor-amyloid-beta1-42 hybrid device for signal amplified detection of MMP-9. Anal Chem 91(13):8252–8258. https://doi.org/10.1021/acs.analchem.9b00926
20. Zhang R, Rejeeth C, Xu W, Zhu C, Liu X, Wan J, Jiang M, Qian K (2019) Label-free electrochemical sensor for CD44 by ligand-protein interaction. Anal Chem 91(11):7078–7085. https://doi.org/10.1021/acs.analchem.8b05966
21. Liu W, Sun S, Huang Y, Wang R, Xu J, Liu X, Qian K (2020) Label-free detection of transferrin receptor by a designed ligand-

protein sensor. Chem Asian J 15(1):56–60. https://doi.org/10.1002/asia.201901512
22. Rejeeth C, Pang X, Zhang R, Xu W, Sun X, Liu B, Lou J, Wan J, Gu H, Yan W, Qian K (2018) Extraction, detection, and profiling of serum biomarkers using designed Fe_3O_4@SiO_2@HA core–shell particles. Nano Res 11(1):68–79. https://doi.org/10.1007/s12274-017-1591-6
23. Hu Y, Qian K, Yuan P, Wang Y, Yu C (2011) Synthesis of large-pore periodic mesoporous organosilica. Mater Lett 65(1):21–23. https://doi.org/10.1016/j.matlet.2010.08.078
24. Gan J, Wei X, Li Y, Wu J, Qian K, Liu B (2015) Designer SiO_2@Au nanoshells towards sensitive and selective detection of small molecules in laser desorption ionization mass spectrometry. Nanomedicine 11(7):1715–1723. https://doi.org/10.1016/j.nano.2015.06.010
25. Huang Y (2007) Pharmacogenetics/genomics of membrane transporters in cancer chemotherapy. Cancer Metastasis Rev 26(1):183–201. https://doi.org/10.1007/s10555-007-9050-6
26. Ahmad R, Mahmoudi T, Ahn MS, Hahn YB (2018) Recent advances in nanowires-based field-effect transistors for biological sensor applications. Biosens Bioelectron 100:312–325. https://doi.org/10.1016/j.bios.2017.09.024
27. Liu J, Chen X, Wang Q, Xiao M, Zhong D, Sun W, Zhang G, Zhang Z (2019) Ultrasensitive monolayer MoS_2 field-effect transistor based DNA sensors for screening of down syndrome. Nano Lett 19(3):1437–1444. https://doi.org/10.1021/acs.nanolett.8b03818
28. Yu Y, Li Y-T, Jin D, Yang F, Wu D, Xiao M-M, Zhang H, Zhang Z-Y, Zhang G-J (2019) Electrical and label-free quantification of exosomes with a reduced graphene oxide field effect transistor biosensor. Anal Chem 91(16):10679–10686. https://doi.org/10.1021/acs.analchem.9b01950
29. Song Y, Luo Y, Zhu C, Li H, Du D, Lin Y (2016) Recent advances in electrochemical biosensors based on graphene two-dimensional nanomaterials. Biosens Bioelectron 76:195–212. https://doi.org/10.1016/j.bios.2015.07.002
30. Wang L, Wang Y, Wong JI, Palacios T, Kong J, Yang HY (2014) Functionalized MoS_2 nanosheet-based field-effect biosensor for label-free sensitive detection of cancer marker proteins in solution. Small 10(6):1101–1105. https://doi.org/10.1002/smll.201302081
31. Park H, Han G, Lee SW, Lee H, Jeong SH, Naqi M, AlMutairi A, Kim YJ, Lee J, Kim WJ, Kim S, Yoon Y, Yoo G (2017) Label-free and recalibrated multilayer MoS_2 biosensor for point-of-care diagnostics. ACS Appl Mater Interfaces 9(50):43490–43497. https://doi.org/10.1021/acsami.7b14479
32. An JH, Park SJ, Kwon OS, Bae J, Jang J (2013) High-performance flexible graphene aptasensor for mercury detection in mussels. ACS Nano 7(12):10563–10571. https://doi.org/10.1021/nn402702w
33. Wang Z, Yi K, Lin Q, Yang L, Chen X, Chen H, Liu Y, Wei D (2019) Free radical sensors based on inner-cutting graphene field-effect transistors. Nat Commun 10(1):1544. https://doi.org/10.1038/s41467-019-09573-4
34. Bolotsky A, Butler D, Dong C, Gerace K, Glavin NR, Muratore C, Robinson JA, Ebrahimi A (2019) Two-dimensional materials in biosensing and healthcare: from in vitro diagnostics to optogenetics and beyond. ACS Nano 13(9):9781–9810. https://doi.org/10.1021/acsnano.9b03632
35. Lee HW, Kang D-H, Cho JH, Lee S, Jun D-H, Park J-H (2018) Highly sensitive and reusable membraneless field-effect transistor (FET)-type tungsten diselenide (WSe_2) biosensors. ACS Appl Mater Interfaces 10(21):17639–17645. https://doi.org/10.1021/acsami.8b03432
36. Sarkar D, Liu W, Xie X, Anselmo AC, Mitragotri S, Banerjee K (2014) MoS_2 field-effect transistor for next-generation label-free biosensors. ACS Nano 8(4):3992–4003. https://doi.org/10.1021/nn5009148
37. Lu C, Hou T, Pan T (2018) High-performance double-gate α-InGaZnO ISFET pH sensor using a HfO_2 gate dielectric. IEEE Trans Electron Devices 65(1):237–242. https://doi.org/10.1109/TED.2017.2776144
38. Kovačević G, Pivac B (2014) Structure, defects, and strain in silicon-silicon oxide interfaces. J Appl Phys 115(4):043531. https://doi.org/10.1063/1.4862809
39. Murugathas T, Zheng HY, Colbert D, Kralicek AV, Carraher C, Plank NOV (2019) Biosensing with insect odorant receptor nanodiscs and carbon nanotube field-effect transistors. ACS Appl Mater Interfaces 11(9):9530–9538. https://doi.org/10.1021/acsami.8b19433
40. Li YT, Jin X, Tang L, Lv WL, Xiao MM, Zhang ZY, Gao C, Zhang GJ (2019) Receptor-mediated field effect transistor biosensor for real-time monitoring of glutamate release from primary hippocampal neurons. Anal Chem 91(13):8229–8236. https://doi.org/10.1021/acs.analchem.9b00832
41. Lu G, Ocola LE, Chen J (2009) Reduced graphene oxide for room-temperature gas sensors. Nanotechnology 20(44):445502. https://doi.org/10.1088/0957-4484/20/44/445502
42. Cai B, Wang S, Huang L, Ning Y, Zhang Z, Zhang G-J (2014) Ultrasensitive label-free detection of PNA–DNA hybridization by reduced graphene oxide field-effect transistor biosensor. ACS Nano 8(3):2632–2638. https://doi.org/10.1021/nn4063424
43. Xu S, Zhan J, Man B, Jiang S, Yue W, Gao S, Guo C, Liu H, Li Z, Wang J, Zhou Y (2017) Real-time teliable determination of binding kinetics of DNA hybridization using a multi-channel graphene biosensor. Nat Commun 8(1):14902. https://doi.org/10.1038/ncomms14902
44. Teo WZ, Chng ELK, Sofer Z, Pumera M (2014) Cytotoxicity of exfoliated transition-metal dichalcogenides (MoS_2, WS_2, and WSe_2) is lower than that of graphene and its analogues. Chem Eur J 20(31):9627–9632. https://doi.org/10.1002/chem.201402680
45. Latiff NM, Sofer Z, Fisher AC, Pumera M (2017) Cytotoxicity of exfoliated layered vanadium dichalcogenides. Chem Eur J 23(3):684–690. https://doi.org/10.1002/chem.201604430
46. Chia HL, Latiff NM, Sofer Z, Pumera M (2018) Cytotoxicity of group 5 transition metal ditellurides (MTe2; M=V, Nb, Ta). Chem Eur J 24(1):206–211. https://doi.org/10.1002/chem.201704316
47. Xu S, Li D, Wu P (2015) One-pot, facile, and versatile synthesis of monolayer MoS2/WS2 quantum dots as bioimaging probes and efficient electrocatalysts for hydrogen evolution reaction. Adv Funct Mater 25(7):1127–1136. https://doi.org/10.1002/adfm.201403863
48. Huang J, He Y, Jin J, Li Y, Dong Z, Li R (2014) A novel glucose sensor based on MoS2 nanosheet functionalized with Ni nanoparticles. Electrochim Acta 136:41–46. https://doi.org/10.1016/j.electacta.2014.05.070
49. Wang K, Wang J, Fan J, Lotya M, O'Neill A, Fox D, Feng Y, Zhang X, Jiang B, Zhao Q, Zhang H, Coleman JN, Zhang L, Blau WJ (2013) Ultrafast saturable absorption of two-dimensional MoS2 nanosheets. ACS Nano 7(10):9260–9267. https://doi.org/10.1021/nn403886t
50. Gan X, Zhao H, Quan X (2017) Two-dimensional MoS2: a promising building block for biosensors. Biosens Bioelectron 89:56–71. https://doi.org/10.1016/j.bios.2016.03.042
51. Sim DM, Kim M, Yim S, Choi M-J, Choi J, Yoo S, Jung YS (2015) Controlled doping of vacancy-containing few-layer MoS_2 via highly stable thiol-based molecular chemisorption. ACS Nano 9(12):12115–12123. https://doi.org/10.1021/acsnano.5b05173
52. Yoo G, Park H, Kim M, Song WG, Jeong S, Kim MH, Lee H, Lee SW, Hong YK, Lee MG, Lee S, Kim S (2016) Real-time electrical detection of epidermal skin MoS_2 biosensor for point-of-care diagnostics. Nano Res 10(3):767–775. https://doi.org/10.1007/s12274-016-1289-1

53. Lee J, Dak P, Lee Y, Park H, Choi W, Alam MA, Kim S (2014) Two-dimensional layered MoS_2 biosensors enable highly sensitive detection of biomolecules. Sci Rep 4(1):7352. https://doi.org/10.1038/srep07352
54. Ayari A, Cobas E, Ogundadegbe O, Fuhrer MS (2007) Realization and electrical characterization of ultrathin crystals of layered transition-metal Dichalcogenides. J Appl Phys 101(1):014507. https://doi.org/10.1063/1.2407388
55. Huang Y, Zheng W, Qiu Y, Hu P (2016) Effects of organic molecules with different structures and absorption bandwidth on modulating photoresponse of MoS_2 photodetector. ACS Appl Mater Interfaces 8(35):23362–23370. https://doi.org/10.1021/acsami.6b06968
56. Sarkar D, Xie X, Kang J, Zhang H, Liu W, Navarrete J, Moskovits M, Banerjee K (2015) Functionalization of transition metal dichalcogenides with metallic nanoparticles: implications for doping and gas-sensing. Nano Lett 15(5):2852–2862. https://doi.org/10.1021/nl504454u
57. Hao Z, Zhu Y, Wang X, Rotti PG, DiMarco C, Tyler SR, Zhao X, Engelhardt JF, Hone J, Lin Q (2017) Real-time monitoring of insulin using a graphene field-effect transistor aptameric nanosensor. ACS Appl Mater Interfaces 9(33):27504–27511. https://doi.org/10.1021/acsami.7b07684
58. Wang X, Hao Z, Olsen TR, Zhang W, Lin Q (2019) Measurements of aptamer-protein binding kinetics using graphene field-effect transistors. Nanoscale 11(26):12573–12581. https://doi.org/10.1039/c9nr02797a
59. Li Z, Ye R, Feng R, Kang Y, Zhu X, Tour JM, Fang Z (2015) Graphene quantum dots doping of MoS2 monolayers. Adv Mater 27(35):5235–5240. https://doi.org/10.1002/adma.201501888
60. Wu S, Zeng Y, Zeng X, Wang S, Hu Y, Wang W, Yin S, Zhou G, Jin W, Ren T, Guo Z, Lu J (2019) High-performance p-type MoS 2 field-effect transistor by toroidal-magnetic-field controlled oxygen plasma doping. 2D Materials 6(2):025007. https://doi.org/10.1088/2053-1583/aafe2d
61. Soleymani J, Hasanzadeh M, Somi MH, Shadjou N, Jouyban A (2019) Highly sensitive and specific cytosensing of HT 29 colorectal cancer cells using folic acid functionalized-KCC-1 nanoparticles. Biosens Bioelectron 132:122–131. https://doi.org/10.1016/j.bios.2019.02.052
62. Huang YW, Wu CS, Chuang CK, Pang ST, Pan TM, Yang YS, Ko FH (2013) Real-time and label-free detection of the prostate-specific antigen in human serum by a polycrystalline silicon nanowire field-effect transistor biosensor. Anal Chem 85(16):7912–7918. https://doi.org/10.1021/ac401610s
63. Xu G, Abbott J, Qin L, Yeung KYM, Song Y, Yoon H, Kong J, Ham D (2014) Electrophoretic and field-effect graphene for all-electrical DNA array technology. Nat Commun 5(1):4866. https://doi.org/10.1038/ncomms5866
64. Ohno Y, Maehashi K, Matsumoto K (2010) Label-free biosensors based on aptamer-modified graphene field-effect transistors. J Am Chem Soc 132(51):18012–18013. https://doi.org/10.1021/ja108127r
65. Chen C, Ke J, Zhou XE, Yi W, Brunzelle JS, Li J, Yong E-L, Xu HE, Melcher K (2013) Structural basis for molecular recognition of folic acid by folate receptors. Nature 500(7463):486–489. https://doi.org/10.1038/nature12327
66. Zhang R, Le B, Xu W, Guo K, Sun X, Su H, Huang L, Huang J, Shen T, Liao T, Liang Y, Zhang JXJ, Dai H, Qian K (2019) Magnetic "squashing" of circulating tumor cells on plasmonic substrates for ultrasensitive NIR fluorescence detection. Small Methods 3(2):1800474. https://doi.org/10.1002/smtd.201800474
67. Sun S, Wang R, Huang Y, Xu J, Yao K, Liu W, Cao Y, Qian K (2019) Design of hierarchical beads for efficient label-free cell capture. Small 15(34):1902441. https://doi.org/10.1002/smll.201902441
68. Wu J, Wei X, Gan J, Huang L, Shen T, Lou J, Liu B, Zhang JX, Qian K (2016) Multifunctional magnetic particles for combined circulating tumor cells isolation and cellular metabolism detection. Adv Funct Mater 26(22):4016–4025. https://doi.org/10.1002/adfm.201504184